JBC RESEARCH ARTICLE

Molecular basis for coordinating secondary metabolite production by bacterial and plant signaling molecules

Received for publication, March 25, 2022, and in revised form, May 3, 2022 Published, Papers in Press, May 11, 2022,
https://doi.org/10.1016/j.jbc.2022.102027

Nannan Zhang[1,2,*,‡], **Jin Wu**[1,3,‡], **Siping Zhang**[4,‡], **Maoran Yuan**[1,3], **Hang Xu**[4], **Jie Li**[1,3], **Pingping Zhang**[1,2], **Mingzhu Wang**[1,3], **Megan L. Kempher**[5], **Xuanyu Tao**[5], **Li-Qun Zhang**[6], **Honghua Ge**[1,3,*], **and Yong-Xing He**[4,*]

From the [1]*School of Life Sciences, Anhui University, Hefei, P.R. China;* [2]*Key Laboratory of Human Microenvironment and Precision Medicine of Anhui Higher Education Institutes, and* [3]*Information Materials and Intelligent Sensing Laboratory of Anhui Province, Institutes of Material Science and Information Technology, Anhui University, Hefei, Anhui, P.R. China;* [4]*Ministry of Education Key Laboratory of Cell Activities and Stress Adaptations, School of Life Sciences, Lanzhou University, Lanzhou, P.R. China;* [5]*Institute for Environmental Genomics, Department of Microbiology and Plant Biology, and School of Civil Engineering and Environmental Sciences, University of Oklahoma, Norman, Ok, USA;* [6]*College of Plant Protection, China Agricultural University, Beijing, P.R. China*

Edited by Karen Fleming

The production of secondary metabolites is a major mechanism used by beneficial rhizobacteria to antagonize plant pathogens. These bacteria have evolved to coordinate the production of different secondary metabolites due to the heavy metabolic burden imposed by secondary metabolism. However, for most secondary metabolites produced by bacteria, it is not known how their biosynthesis is coordinated. Here, we showed that PhlH from the rhizobacterium *Pseudomonas fluorescens* is a TetR-family regulator coordinating the expression of enzymes related to the biosynthesis of several secondary metabolites, including 2,4-diacetylphloroglucinol (2,4-DAPG), mupirocin, and pyoverdine. We present structures of PhlH in both its apo form and 2,4-DAPG-bound form and elucidate its ligand-recognizing and allosteric switching mechanisms. Moreover, we found that dissociation of 2,4-DAPG from the ligand-binding domain of PhlH was sufficient to allosterically trigger a pendulum-like movement of the DNA-binding domains within the PhlH dimer, leading to a closed-to-open conformational transition. Finally, molecular dynamics simulations confirmed that two distinct conformational states were stabilized by specific hydrogen bonding interactions and that disruption of these hydrogen bonds had profound effects on the conformational transition. Our findings not only reveal a well-conserved route of allosteric signal transduction in TetR-family regulators but also provide novel mechanistic insights into bacterial metabolic coregulation.

With the increasing demand for crop production, contamination of soil and water by chemical fertilizers and pesticides has become a challenging global environmental problem (1). The use of plant growth–promoting rhizobacteria (PGPR), which are biocontrol agents that colonize plant roots and suppress the growth of phytopathogens, has been proven to be an environment-friendly and sustainable way of increasing crop yields (2, 3). The production of secondary metabolites, such as antibiotics and siderophores, is a major mechanism used by PGPR to antagonize plant pathogens (4, 5). Typically, a PGPR strain has the potential to produce multiple secondary metabolites *via* distinct metabolic pathways involving different gene clusters. As secondary metabolism is a very energy-consuming process and exerts a fitness cost to the producers, spontaneous mutants that do not secrete the secondary metabolites can invade the population by outcompeting the WT strains and eventually lead to the population collapse (6). To circumvent this problem, bacteria usually coordinate the biosynthetic processes of different secondary metabolites in response to their physiological status and various environmental cues, *i.e.*, promote the coproduction of certain secondary metabolites while inhibiting the production of another (7). In this way, bacteria can save its energy by only producing the secondary metabolites that are useful at a specific time, thereby preventing the invasion of the secondary metabolite nonproducing mutants and maintaining the stability of the whole bacterial population. However, in most cases, it is not very clear how PGPR coordinates the production of different secondary metabolites, and a better understanding of this process will aid in designing and developing more effective and potent biocontrol agents in agricultural practice.

Pseudomonas fluorescens is a well-known PGPR that antagonizes invading phytopathogens by producing a wide array of secondary metabolites such as 2,4-diacetylphloroglucinol (2,4-DAPG), mupirocin, pyoluteorin, pyrrolnitrin, rhizoxin analogs, orfamide A, hydrogen cyanide, and pyoverdine (4, 8). Most of these metabolites are synthesized in response to cell densities through bacterial cell–cell communication (9). Positive feedback regulation *via* autoinducers is a hallmark of this cooperative bacterial behavior, and acyl-homoserine lactone-based quorum sensing has been shown to take a part in the biosynthesis of certain secondary metabolites (8, 10). More importantly, the GacA/GacS two-component system plays a

‡ These authors contributed equally to this work.
* For correspondence: Nannan Zhang, zhangnn@ahu.edu.cn; Honghua Ge, hhge@ahu.edu.cn; Yong-Xing He, heyx@lzu.edu.cn.

major role in posttranscriptionally regulating the production of secondary metabolites of *P. fluorescens*, although the inducing signal of GacA/GacS is still unknown (11, 12). Metabolic coregulation has been reported to operate between the 2,4-DAPG and pyoluteorin biosynthesis, but the coordination mechanism for the production of other secondary metabolites is still not well understood.

Among the diverse secondary metabolites produced by *P. fluorescens*, 2,4-DAPG is a major contributor to the suppression of soil-borne pathogens including *Fusarium oxysporum*, *Septoria tritici*, *Thielaviopsis basicola*, and *Rhizoctonia solani* (13, 14). Two pairs of oppositely transcribed operons, *phlF-phlACBDE* and *phlG-phlH*, are involved in 2,4-DAPG biosynthesis (15). The *phlABCD* gene cluster encodes catalytic enzymes that convert malonyl-CoA into 2,4-DAPG through multiple steps (16, 17), while *phlE* encodes a transmembrane permease implicated in 2,4-DAPG resistance (18). The TetR-family regulator PhlF transcriptionally represses the expression of the 2,4-DAPG biosynthetic operon *phlACBDE*, and this repression is released by 2,4-DAPG, resulting in the positive-feedback regulation of 2,4-DAPG biosynthesis (19). The PhlH regulator, which also belongs to the TetR family, regulates the expression of the 2,4-DAPG hydrolase *phlG* in response to 2,4-DAPG, thus providing a negative-feedback regulation of 2,4-DAPG biosynthesis (20). This regulatory mechanism is likely to be crucial for the competitive root colonization of *P. fluorescens*, since triggering 2,4-DAPG degradation in response to its intracellular concentration could relieve the metabolic burden caused by 2,4-DAPG biosynthesis (21).

Like other TetR-family regulators, PhlH contains an N-terminal DNA-binding domain (DBD) and a larger C-terminal ligand-binding domain (LBD). In contrast to the conserved DBD, the LBD of PhlH exhibits little sequence identity with other well-characterized TetR-family regulators, consistent with the notion that the ligands sensed by TetR-family regulators show considerable diversity. More recently, PhlH was also found to recognize several plant-derived flavonoids including phloretin, which reduced the production of 2,4-DAPG in *P. fluorescens* (21). Therefore, it appears that PhlH can sense molecular signals from both bacteria and plants and precisely balance the costs and benefits of 2,4-DAPG production in complex and dynamic niches. However, little is known regarding the mechanism on how PhlH recognizes its cognate molecular signals and what the physiological consequences of these signals are. Here using quantitative proteomics, we found the TetR-family regulator PhlH from *P. fluorescens* was involved in coordinating the expression of proteins involved in the biosynthesis of 2,4-DAPG, mupirocin, and pyoverdine. More importantly, we presented the crystal structures of *P. fluorescens* PhlH in both its apo form and 2,4-DAPG–bound form, illustrating its ligand-recognizing and allosteric switching mechanisms. Our work not only reveals a novel role of PhlH in coordinating different secondary metabolic pathways but provides important mechanistic insights into the ligand-triggered conformational switching of TetR-family regulators.

Results

PhlH influences the expression of proteins involved in biosynthesis of the secondary metabolites 2,4-DAPG, mupirocin and pyoverdine

To explore the physiological role of PhlH, we performed quantitative protein expression profiling of the WT and *phlH* in-frame deletion mutant (Δ*phlH*) strains. Differentially expressed proteins were screened based on the criteria of fold change greater than 1.5 and *p*-value less than 0.05, leading to the identification of 29 upregulated and 45 downregulated proteins in the Δ*phlH* strain (Fig. 1*A* and Table S1). Based on Gene Ontology enrichment analysis, differentially expressed proteins involved in antibiotic biosynthesis and porin activity were significantly enriched ($p < 0.010$; Fisher's exact test) in Δ*phlH* (Fig. 1*B*). The expression of the DAPG hydrolase PhlG increased over 32-fold in the Δ*phlH* strain compared to the WT strain, consistent with our previous finding that PhlH acts as a repressor of the *phlG* gene (20). Interestingly, proteins involved in pyoverdine biosynthesis including PvdA, PvdD, PvdE, PvdH, PvdL, and MbtH (22, 23) were upregulated in the Δ*phlH* strain, though to a lesser extent. In addition, the Δ*phlH* strain showed decreased expression of an acyl-CoA dehydrogenase implicated in catalyzing a step of fatty acid β-oxidation (24) and 12 proteins involved in mupirocin biosynthesis, including MmpA, MmpC, MmpD, MupC, MupE, MupJ, MupK, MupP, MupQ, MupV, MupW, and MupZ(8); however, these proteins only had fold changes around 1.5, suggesting that PhlH indirectly influence fatty acid β-oxidation and production of pyoverdine and mupirocin.

Overall structure and ligand-binding tunnel of PhlH

To investigate how PhlH recognizes its cognate ligands, we solved the crystal structure of PhlH in a complex with 2,4-DAPG at 2.1 Å resolution. Similar to typical TetR-family regulators, PhlH forms a homodimer with each subunit consisting of a DBD (helices α1-α3) and an LBD (helices α4-α9). The DBD of PhlH contains a canonical DNA-binding helix-turn-helix motif (helices α2 and α3) with the α3 helix recognizing DNA. The two LBDs mediate dimerization through the α6 helix and α8-α9 helices, which form a 4-helix bundle in the dimer. A DALI search revealed that PhlH has the highest structural similarity with phloretin-bound TtgR from *Pseudomonas putida* (PDB code: 2UXI), with a Z-score of 5.8 and root mean square deviation (RMSD) of 4.44 Å for the 268 equivalent Cα positions, despite the fact that PhlH shares little sequence identity (∼18%) with TtgR. Notably, the distance between the DNA recognition helices (α3, residues 54–57) is ∼46 Å, which is significantly larger than the 34 Å major groove distance of B-DNA, confirming that 2,4-DAPG is an allosteric ligand precluding PhlH from binding DNA.

A prominent feature of PhlH is a long interior tunnel-like cavity, surrounded by helices α4, α5, α6, α7, and α8, in a vertical orientation with respect to the axis of the dimer (Fig. 2*A*). The tunnel is ∼30 Å long and fully buried, with mainly hydrophobic residues lining the tunnel and pointing their side chains toward the lumen. The ligands 2,4-DAPG are

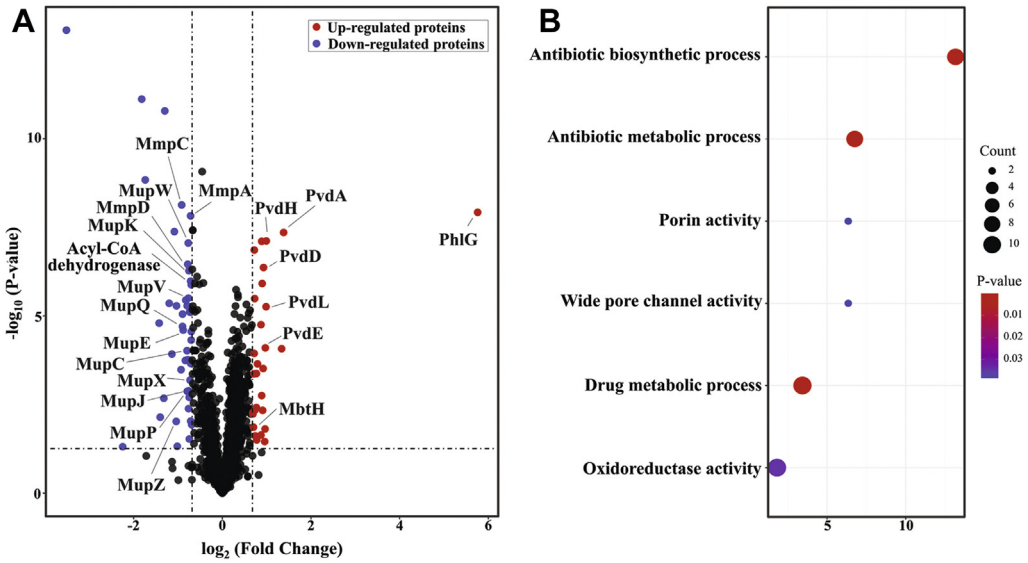

Figure 1. *Pseudomonas fluorescens* PhlH as a TetR-family regulator controls the transcriptional regulation of biosynthesis of the secondary metabolites 2,4-DAPG, mupirocin, and pyoverdine. *A*, comparative proteomic analysis of the WT and Δ*phlH* strains. A volcano plot showing the differentially expressed proteins in the Δ*phlH* strain compared with the WT strain. The *red* and *blue* spots indicate upregulated and downregulated proteins, respectively. B, *GO* enrichment analysis of the differentially expressed proteins in the Δ*phlH* strain. The enriched GO terms with $p < 0.05$ were displayed. 2,4-DAPG, 2,4-diacetylphloroglucinol; GO, Gene Ontology.

well-defined and located at both ends of the tunnel. Consistent with the hydrophobic nature of 2,4-DAPG, all residues involved in 2,4-DAPG binding are hydrophobic, including V80, L85, A145, L148, A169, and F173 in the α4, α7, and α8 helices from one protomer and F178′, L186′, V190′ in the α8 helix in the other protomer (Fig. 2*B*). Of note, the residue F173 interacts with 2,4-DAPG *via* π-π stacking, which could be essential for the binding affinity between PhlH and 2,4-DAPG.

The fact that the interior tunnel of PhlH is not fully occupied by 2,4-DAPG suggests that PhlH should have the potential to accommodate other hydrophobic ligands of larger sizes. Indeed, PhlH was recently reported to recognize several plant-derived flavonoids including phloretin (21). Despite multiple attempts, no cocrystals of PhlH and flavonoids were obtained. Instead, we used the molecular docking method to interrogate the interaction mode of PhlH and phloretin

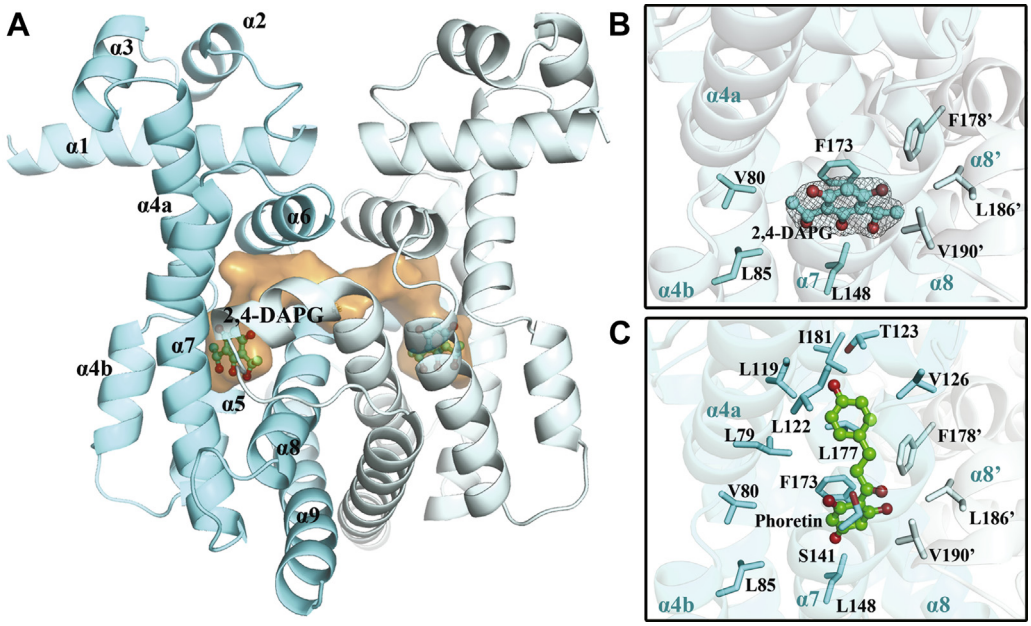

Figure 2. Structure of PhlH in complex with 2,4-DAPG. *A*, cartoon representation of PhlH in complex with 2,4-DAPG. The two protomers are colored in *cyan* and *light cyan*, respectively, with the bound 2,4-DAPG shown in *sticks*. The ligand-binding tunnel is the hydrophobic tunnel in ligands recognition and colored in *orange*. B, a close-up view of the 2,4-DAPG binding site and residues in the vicinity of 2,4-DAPG (colored in *cyan*) are shown in *sticks*. The electron density around 2,4-DAPG is colored *gray* and contoured at 1.0 σ. *C*, a closed-up view of the interaction mode between PhlH and the docked phloretin (colored in *green*). 2,4-DAPG, 2,4-diacetylphloroglucinol.

(Fig. 2*C*). It was revealed that the phloroglucinol moiety of phloretin almost overlapped with the 2,4-DAPG molecule, suggesting a very similar binding mode shared between phloretin and 2,4-DAPG. However, as the phloroglucinol moiety lacks two acetyl groups compared to 2,4-DAPG, it makes fewer contacts with the hydrophobic residues involved in 2,4-DAPG binding, including F173, L186, and V190. This may explain the weaker binding affinity of phloretin with PhlH compared to 2,4-DAPG (21). In addition, the phenol moiety of phloretin points to the interior of the PhlH ligand-binding tunnel, making contact with L119, L122, L177, and I181, due to the long, hydrophobic nature of the PhlH interior tunnel.

The ligand-binding tunnel is essential for the ligand-induced dissociation of the PhlH–DNA complex

To evaluate the role of the hydrophobic ligand-binding tunnel in PhlH–DNA association, single-site mutants of the ligand-binding residues (V80A, L85A, L148A, F173A, F178A, L186A, and V190A) were constructed, and electrophoretic mobility shift assays (EMSAs) were performed to monitor the ligand-induced protein–DNA dissociation. Mutated residues involved in ligand binding can decrease the affinity of PhlH and a ligand, thus leading to the increased strength of PhlH–DNA interactions in the presence of ligands. As shown in Figure 3, the L85A, L186A, F173A, and V190A mutants displayed increased binding affinities to the *phlG* operator sequence in the presence of 2,4-DAPG, indicating that these four residues are important for binding 2,4-DAPG. Using isothermal titration calorimetry (ITC) assay, it was further confirmed that these mutants had significantly reduced binding affinities toward 2,4-DAPG compared to the WT PhlH (Table 1 and Fig. S1). For the V80A, L148A, and F178A mutants, 2,4-DAPG could still trigger protein–DNA unbinding, but to a lesser extent, compared with the case of the WT PhlH, suggesting these three residues played a less prominent role in binding 2,4-DAPG. On the other hand, phloretin showed little induction of DNA dissociation for the L85A and L186A mutants and slightly compromised induction effects for the V80A and L148A mutants (Fig. 3), supporting our docking result that phloretin and 2,4-DAPG occupy the same hydrophobic tunnel of PhlH. However, the F173A and V190A mutants still showed phloretin-induced DNA dissociation, consistent with the docking result that these two residues had weaker interactions with phloretin than with 2,4-DAPG. Interestingly, phloretin barely induced DNA dissociation from the F178 mutant, indicating that the F178 residue plays a more significant role in binding phloretin than 2,4-DAPG. Collectively, these results confirmed that the ligand-binding tunnel is essential for ligand-induced DNA dissociation from PhlH but also suggested slightly different binding modes for different ligands such as 2,4-DAPG and phloretin.

Structural comparison of the apo-PhlH and 2,4-DAPG-bound-PhlH

To unravel the ligand-induced allosteric switching mechanism of PhlH, we solved the crystal structure of PhlH in the apo form at 2.4 Å resolution. Superposition of the apo-PhlH and 2,4-DAPG-bound PhlH dimers resulted in an RMSD of 3.0 Å for 306 Cα atoms, indicating a large conformational change between these two structures (Fig. 4*A*). A further inspection revealed that the LBD showed a much larger conformational change than the DBD (RMSD of 0.7 Å for 97 Cα atoms *versus* 0.28 Å for 42 Cα atoms) upon 2,4-DAPG binding (Fig. 4*B*). In the absence of 2,4-DAPG, the α7 helix and α8 helix which participate in 2,4-DAPG binding were partially unfolded in the N terminus and C terminus, respectively, whereas upon 2,4-DAPG binding, these two helices became intact, well-folded long α helices, this was most likely due to their hydrophobic interaction with 2,4-DAPG *via* residues F173, L186, L191, and V190. It seemed that 2,4-DAPG acted as a hydrophobic core that facilitated proper folding of the α7 and α8 helices, and these helices were essential for 2,4-DAPG

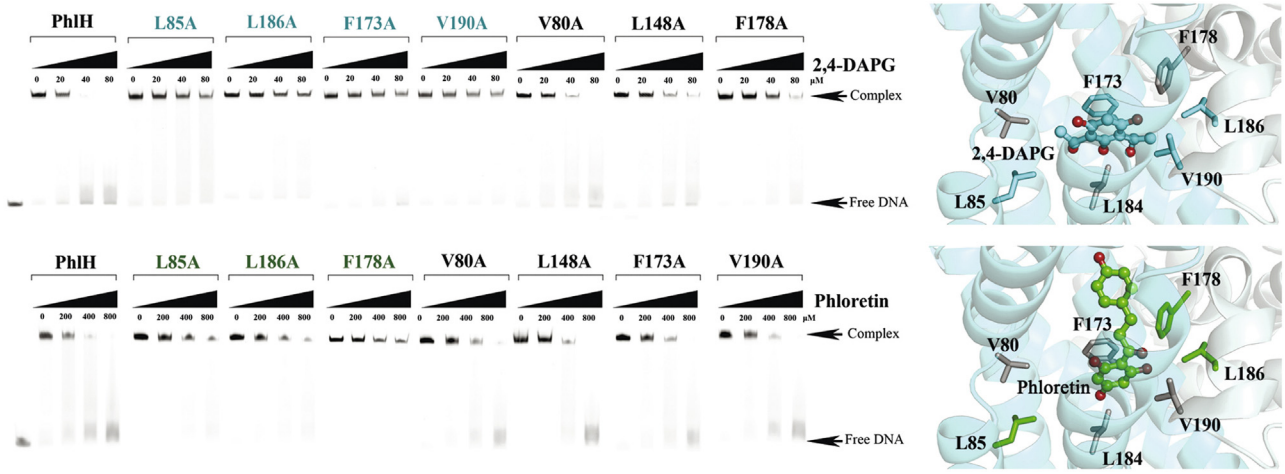

Figure 3. Ligand-induced dissociation of the PhlH–DNA complex results in an open to closed conformational transition of PhlH. Electrophoretic mobility shift assays of the WT PhlH and PhlH mutants (V80A, L85A, L148A, F173A, F178A, L186A, and V190A) with the upstream region of *phlG* (free DNA) in the presence of increasing concentrations (0–80 μM) of 2,4-DAPG (*upper row*) or increasing concentrations (0–800 μM) of phloretin (*bottom row*). The interaction modes between PhlH and 2,4-DAPG/phloretin are shown on the right of separate rows. 2,4-DAPG, 2,4-diacetylphloroglucinol.

Table 1
ITC analysis of the interactions between PhlH mutant proteins and 2,4-DAPG

Protein	K_a (M^{-1})	K_d (μM)	ΔG (kcal mol^{-1})	ΔH (kcal mol^{-1})	$T\Delta S$ (kcal mol^{-1})
PhlH	1.17×10^5	8.5	−6.8	−12.2	−5.4
F173A	4.94×10^4	20.2	−6.5	−44.0	−37.5
L85A	2.56×10^4	39	−6.0	−5.3	0.7
L186A	6.50×10^4	15.4	−6.5	−2.1	4.4
V190A	4.12×10^4	24.3	−6.3	−4.8	1.5
H76A	9.14×10^4	10.9	−6.7	−4.1	2.6
R124A	7.54×104	13.2	−7.0	−34.5	−27.5

binding. Notably, the long α4 helix comprising residues (K64-R91) in the apo-PhlH structure kinked and was drawn closer to 2,4-DAPG in the 2,4-DAPG-bound structure, with residue Val80 forming a hydrophobic interaction with 2,4-DAPG. This led to the displacement of the α4 helix, which acted like a pendulum that forced the DNA recognition helix α3 to move in the same direction. Further analysis of the PhlH dimeric assembly revealed that 2,4-DAPG binding resulted in a larger dimeric interface of ∼2250 $Å^2$, compared with the buried interface of ∼1850 $Å^2$ in the apo structure, indicating 2,4-DAPG binding not only influenced the conformation of the PhlH protomer but had a substantial impact on the mode of dimeric assembly as well. The increased dimeric interface was mostly attributed to tighter α6-α6 packing (Fig. 4*A*), suggesting that the intersubunit coupling was strengthened upon 2,4-DAPG binding. As a consequence, the 2,4-DAPG-bound PhlH dimer displayed a DBD-open conformation, with 46 Å distance between the two DNA recognition helices α3, whereas the apo-PhlH dimer showed a DBD-closed conformation, with the separation distance of the α3 helices perfectly matching the 34 Å separation between the major grooves of an ideal B-DNA (Fig. 4*A*).

The above structural comparison suggests that 2,4-DAPG mechanically triggers a closed to open conformational transition of PhlH. It is intriguing that the ligand-free form of PhlH exhibits a closed, DNA-binding competent configuration, which is in sharp contrast with the previous notion that the vast majority of available TetR-family crystal structures including TetR, with no effector bound, correspond to the open conformation (25–27). For those TetR-family regulators, the presence of cognate operator DNA rather than ligand dissociation induces an open to closed conformational switching. Therefore, PhlH is considerably different from these TetR-family regulators in the aspect that dissociation of 2,4-DAPG from the LBD was sufficient to allosterically trigger a pendulum-like movement of the DBD within the PhlH dimer, leading to a conformational transition from closed to open. Since PhlH adopts two distinct conformations, we speculated that specific hydrogen-bonding interactions may be involved in stabilizing these two separate conformations and may play an important role in the allosteric signal transduction. Consistently, in the 2,4-DAPG bound, DBD-open conformation, the H76 residue in the α4 helix forms a hydrogen bond with K144 in the α7 helix, whereas in the ligand-free, DBD-closed conformation, this interaction was completely disrupted. Additionally, the side-chain of the R124 residue from the α6 helix seems to be involved in maintaining the closed conformation by forming hydrogen bonds with the

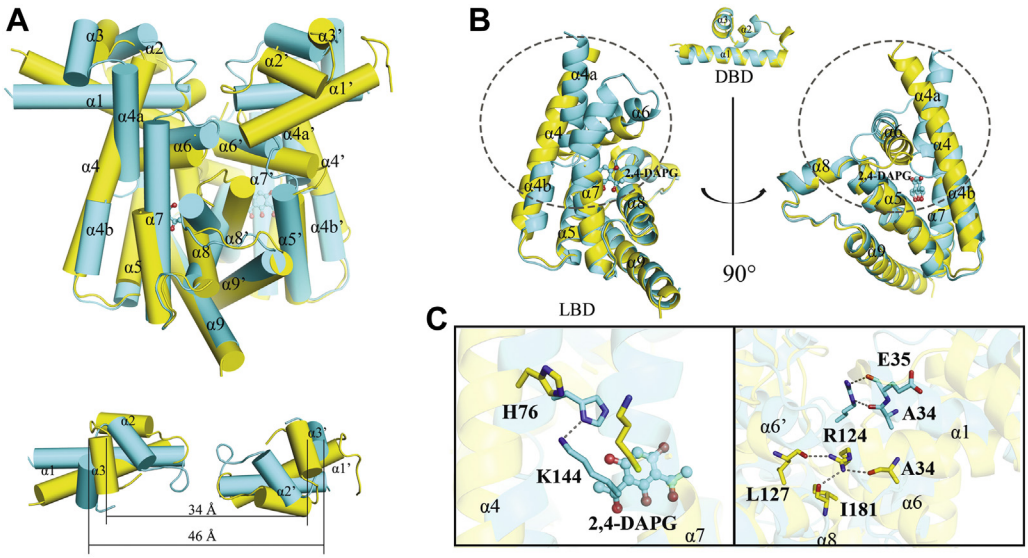

Figure 4. Superposition of apo-PhlH and 2,4-DAPG-bound-PhlH. *A*, comparison of dimer structures of apo-PhlH (*yellow*) and 2,4-DAPG-bound-PhlH (*cyan*). The distances between the DNA recognition helices α3 within the dimer are displayed. *B*, separate superposition of the DBDs and LBDs from the apo-PhlH and 2,4-DAPG-bound-PhlH protomers. The DBDs are well superimposed, whereas the corresponding LBDs show large conformational changes. *C*, changes of the hydrogen bonding interactions in the LBDs from the apo-PhlH and 2,4-DAPG-bound-PhlH. The hydrogen bonds are represented by *black dotted lines*. 2,4-DAPG, 2,4-diacetylphloroglucinol; DBD, DNA-binding domain; LBD, ligand-binding domain.

main-chain carboxyls of A34 from the α1 helix, I181 from the α8 helix, and L127 from the α6′ helix, yet it is dislocated and only forms hydrogen bonds with the main-chain carboxyls of A34 and E35 in the 2,4-DAPG bound, open conformation (Fig. 4*C*). Multiple sequence alignment further indicates the H76, K144, and R124 residues are well-conserved in the PhlH proteins from different *Pseudomonas* species (Fig. S2), suggesting that the abovementioned hydrogen bonding interactions are likely to take an important part in maintaining the ligand-binding and the DNA-binding conformations of PhlH.

Key residues involved in the conformational switching

To investigate the conformational dynamics of PhlH, all atom molecular dynamics (MD) were performed on the structure of 2,4-DAPG-bound PhlH for 1000 ns. To characterize the low-energy conformational states of the simulation system, we computed the potential of mean force (PMF) free energy profiles (Fig. 5). The separation distance between the two DNA recognition helices α3 (dH3), H76:ND1-K144:NZ distance (dHK) were selected as reaction coordinates. The 2D PMF profile revealed a single low-energy state (dH3 = ∼47 Å, dHK= ∼2.8 Å). This conformational state corresponds to the open, DNA binding-incompetent conformation, as indicated by the 47 Å distance between the α3 helices (Fig. 5*A*). In this low-energy state, the hydrogen binding between H76 and K144 is preserved, corroborating our hypothesis that these two residues are essential for locking PhlH in the open conformation. To further explore the dynamics of the conformational transition, we removed the 2,4-DAPG molecule from the structure and performed a 1000 ns MD simulation. Interestingly, the 2D PMF profile revealed an additional low energy state (dH3 = ∼47 Å, dHK= ∼5.0 Å), which corresponds to an intermediate, DNA binding-incompetent state, with the H76-K144 hydrogen-bond interrupted (Fig. 5*B*). This suggests that dissociation of DAPG first results in disruption of the H76-K144 interaction and may subsequently trigger a pendulum-like movement of the DBDs. To sample a larger conformational space of PhlH with 2,4-DAPG removed, we performed a 1000 ns gaussian accelerated molecular dynamics (GaMD), an enhanced sampling computational technique that can accelerate simulations by orders of magnitude (28). Intriguingly, the 2D PMF profile revealed a low energy state (dH3 = ∼38 Å, dHK= ∼5.0 Å) with the interrupted H76-K144 interaction, and the α3 separation distance of this state is quite similar to that of the closed, DNA binding-competent conformation (Fig. 5*C*).

We also performed a 1000 ns MD simulation on the structure of apo-PhlH. The distances of R124:NH1-A34:O (dRA) and dH3 were selected as reaction coordinates to compute the PMF profile, which revealed the lowest energy

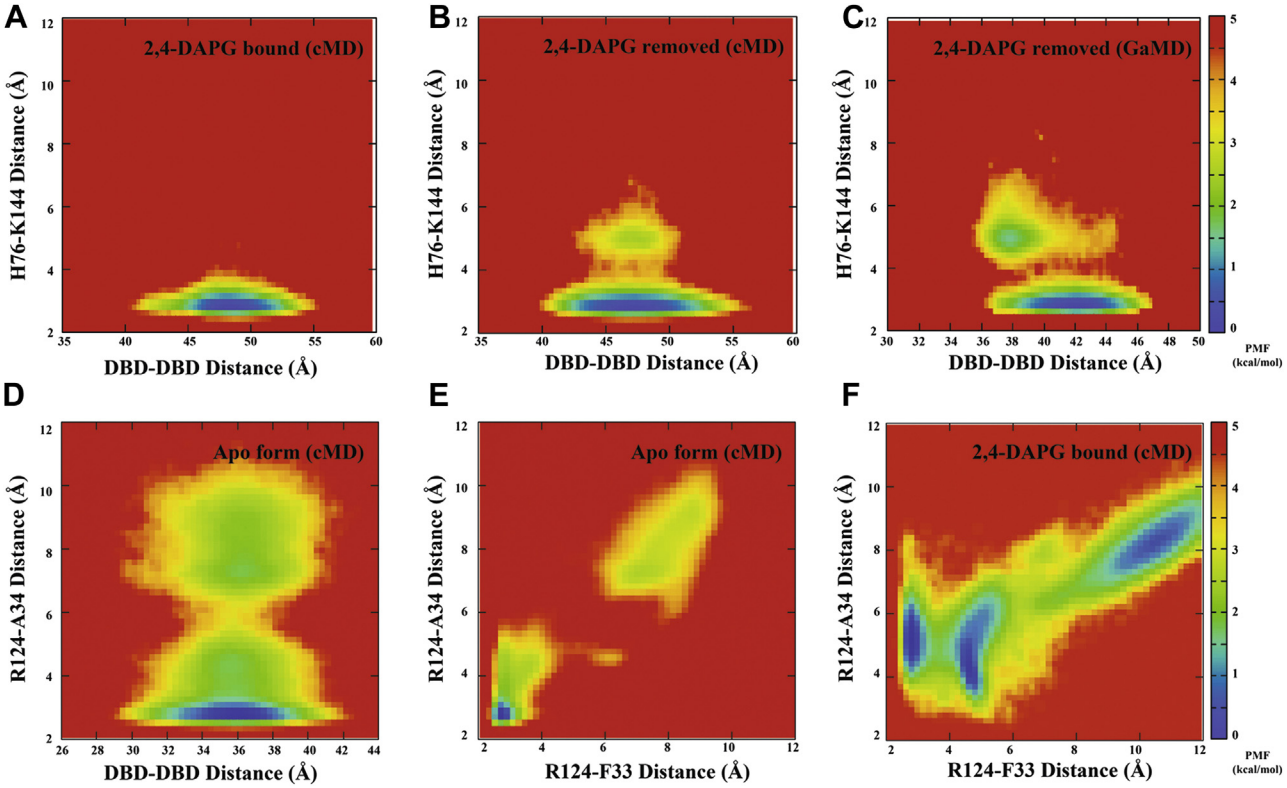

Figure 5. Key residues involved in the conformational switching. 2D PMF profiles of the H76-K144 distance *versus* the DBD-DBD distance from 1000 ns conventional MD (cMD) simulation of the 2,4-DAPG-bound-PhlH dimer (*A*), 1000 ns cMD (*B*), and GaMD (*C*) simulations of the PhlH dimer with 2,4-DAPG removed. *D*, 2D PMF profiles of the R124-A34 distance *versus* the DBD-DBD distance from 1000 ns cMD simulation of the apo-PhlH dimer. 2D PMF profiles of the R124-A34 distance versus the R124-F33 distance from 1000 ns cMD simulation of the apo-PhlH dimer (*E*) and the 2,4-DAPG-bound-PhlH dimer (*F*). 2,4-DAPG, 2,4-diacetylphloroglucinol; MD, molecular dynamics; PMF, potential of mean force.

state (dH3 = ∼36 Å, dRA = ∼2.8 Å), corresponding to the closed, DNA-binding conformation (Fig. 5*D*). Note that the hydrogen bond between R124 and A34 is preserved in this state, confirming its essential role in maintaining the closed conformation. We also monitored the distances of R124:NH1-I181:O (dRI) and R124:NH1-L127:O (dRL) but found these two hydrogen bonds were disrupted in the lowest energy state (Fig. S3). Instead, we found that the distance of R124:NH2-F33:O (dRF) is suitable for hydrogen bond formation in the lowest energy state (dRF = ∼2.8 Å, dRA = ∼2.8 Å) (Fig. 5*E*). In the simulation system of 2,4-DAPG-bound PhlH, both the hydrogen bonds of R124:NH1-A34:O and R124:NH2-F33:O were completely disrupted in the low energy states (Fig. 5*F*). Collectively, our simulation results suggest an important role for the H76-K144, R124-F33 and R124-A34 interactions in the conformational transition of PhlH.

Since the H76-K144 and R124-F33/A34 interactions were implicated in locking PhlH in open and closed conformation, respectively, we reasoned that disruption of the H76-K144 interaction would promote the open to closed conformational change, while disrupting the R124-F33/A34 interaction would promote the closed to open conformational transition, without affecting the ligand-binding affinity. To test this hypothesis, we made the H76A and R124A mutant proteins and monitored the ligand-bind and DNA-binding affinities using ITC and EMSAs assays. It was shown that these two mutations have negligible effects on binding affinities of PhlH with 2,4-DAPG (Fig. 6*A* and Table 1), indicating H76 and R124 are not involved in ligand binding. For the H76 mutant protein, 2,4-DAPG did not effectively induce the protein–DNA dissociation, confirming its role in locking PhlH in the open conformation (Fig. 6*B*). The R124 mutant protein completely lost its DNA-binding ability, corroborating its role in locking PhlH in the closed conformation (Fig. 6*B*). Taken together, these results confirmed H76 and R124 are the key residues for the PhlH conformational switching.

Functional implications for PhlH homologs in diverse bacterial genomes

To investigate the distribution of PhlH homologs in bacteria, we retrieved 1000 homologous sequences from the UniProt database and constructed a sequence similarity network (SSN) using the enzyme similarity tool (29). This analysis showed that the PhlH homologs are mostly distributed in Proteobacteria but are also present in other bacterial phyla such as Acidobacteria, Verrucomicrobia, Planctomycetes, and Firmicutes (Fig. 7*A*). The retrieved sequences also included several PltZ proteins which were characterized to be involved in pyoluteorin biosynthesis by regulating the expression of an ABC transporter (30, 31). We next used the Markov Clustering method (32) to classify these PhlH homologs into several isofunctional sequence clusters (Fig. 7*B*). Since the PltZ and PhlH proteins from *Pseudomonas* species form separate clusters (cluster 4 and cluster 7) distinct from other PhlH homologs, the presented sequence clusters in the PhlH SSN are likely to represent isofunctional protein subfamilies. We then selected a representative sequence from each of the top 13 clusters and performed a multiple sequence alignment, revealing that the LBDs showed much more sequence variability compared with the DBDs (Fig. S4). This suggests that different clusters of PhlH may have the potential to recognize distinct ligands, which is further corroborated by the fact that the ligand-binding residues are variable among members of the different sequence clusters. Genomic context analysis further revealed that most of the PhlH homologs are adjacent to efflux transporters (ABC transporters and AcrB family efflux pumps), which are putatively implicated in resistance to antibiotic or toxic compounds. It is therefore likely that these PhlH homologs could potentially prevent toxic chemicals from accumulating in the cells by controlling the expression of efflux transporters in response to the toxic chemicals. Notably, the residues involved in conformational switchings such as F33, A34, and R124 are almost invariable, suggesting a well-conserved allosteric regulation mechanism among the PhlH homologs (Fig. 8*A*).

Discussion

The TetR-family of regulators constitute a large family of transcription factors involved in diverse prokaryotic signal transduction systems. A typical TetR regulator possesses a C-terminal LBD that functions by perceiving different types of

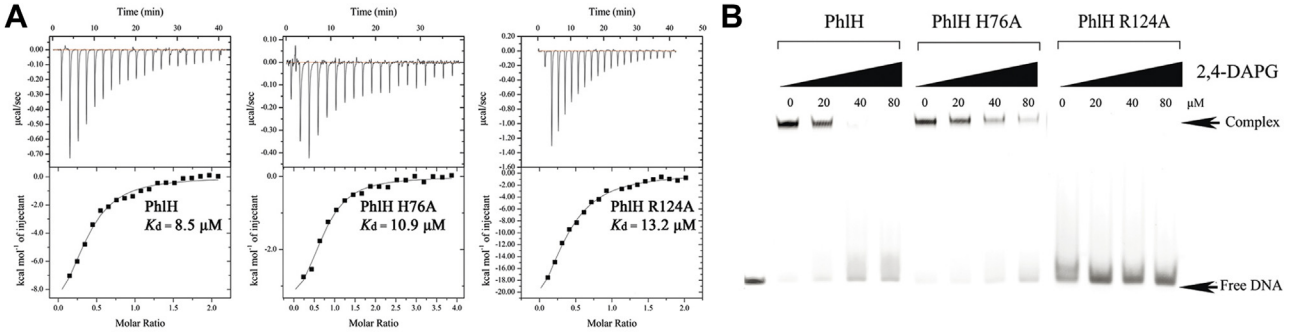

Figure 6. Binding affinity assays of key residues of PhlH involved in the conformational switching. *A*, the binding affinities of PhlH and the mutant proteins (H76A and R124A) with 2,4-DAPG were evaluated using ITC analysis. The binding curves corrected for the dilution effects were fit to a one-site binding model and the *Kd* values were calculated by the NanoAnalyze software. *B*, electrophoretic mobility shift assays of the WT PhlH (from the same WT-PhlH EMSA assay in *upper row* of Fig. 3) and PhlH mutants (H76A and R124A) with fluorescently labeled DNA in the presence of increasing concentrations (0–80 μM) of 2,4-DAPG. 2,4-DAPG, 2,4-diacetylphloroglucinol; EMSA, electrophoretic mobility shift assay; ITC, isothermal titration calorimetry.

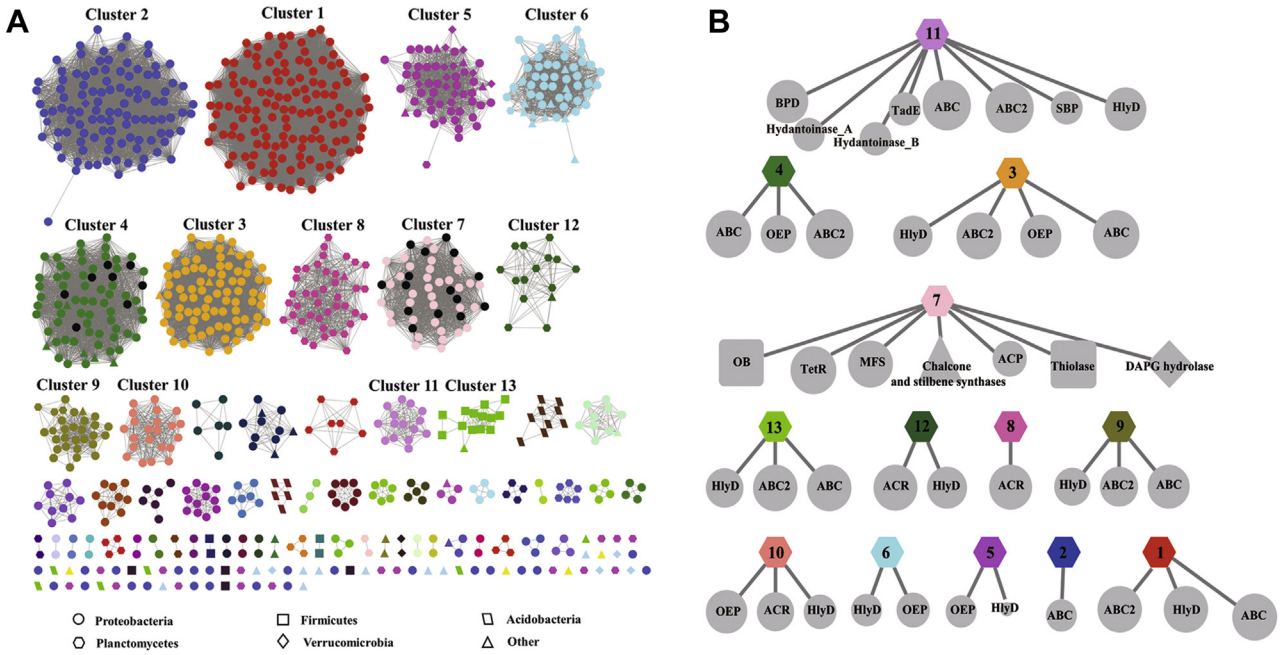

Figure 7. PhlH homologues reveal a conserved conformational switching mechanism of TetR-family regulators. *A*, SSN of 1000 PhlH homologs. The Markov clustering method was used to classify these PhlH homologs into several isofunctional sequence clusters. Nodes from different clusters were colored differently. Different node shapes denote different bacterial phyla. Nodes of characterized PhlH (in cluster 7) and PltZ (in cluster 4) protein sequences are colored in *black*. *B*, Genomic Neighborhood Network with the SSN clusters of PhlH (cluster 1–13) as the hub nodes and Pfam families of the neighboring genes as the spoke nodes. SSN, sequence similarity network.

signals and an N-terminal DBD that serves as an output by regulating the expression of target genes. The LBDs of the TetR regulators are usually more diverse compared with the DBDs and can accommodate a wide array of inducing ligands (26). Here, we illustrated the structural basis of how the TetR regulator PhlH, which possesses an LBD with low homology with any well-characterized TetR regulator, recognizes the bacterial and plant metabolites 2,4-DAPG and phloretin. The crystal structure of PhlH in complex with 2,4-DAPG revealed a long interior tunnel of ∼30 Å long, with mostly hydrophobic residues pointing their side chains toward the lumen. The ligand 2,4-DAPG was fully buried in the tunnel and interacted with several hydrophobic residues, with no hydrogen bonds formed between 2,4-DAPG and PhlH. Through docking and mutagenesis analyses, we demonstrated that the plant flavonoid phloretin shares a very similar binding mode with 2,4-DAPG. As hydrogen bonding typically plays a prominent role in the specificity of protein–ligand recognition (33), the absence of direct hydrogen bonds likely accounts for the promiscuity of PhlH in ligand recognition and the relatively weak ligand-binding affinities (micromolar range). Previous interrogation of other promiscuous TetR-family regulators such as TtgR, QacR, and EthR revealed few hydrogen bonds between the protein and ligands (34–36), the dissociation constants of which were also in the micromolar range. These TetR-family regulators varied substantially in the size of their interior cavity, suggesting that they recognize structurally diverse ligands by probing the ligand shapes, complementarity, and sizes with the interior pockets.

For most TetR-family regulators, the apo-form structures usually adopt open, DNA-binding incompetent conformation, which most closely resembles the ligand-induced conformation (27). Therefore, the allosteric mechanism of TetR regulators is typically illustrated by comparing the DNA-bound and ligand-bound structures of TetR-family proteins. This also suggests that for these TetR-family proteins, an open to closed conformational transition requires not only dissociation of the ligand but also binding to the DNA by the regulators as well. The PhlH regulator, however, is rather different in that dissociation of 2,4-DAPG is sufficient to allosterically trigger the conformational transition. MD simulation and mutagenesis analysis highlighted the importance of the H76-K144 and R124-F33/A34 interactions in conformational switching, suggesting a plausible mechanism for signal transduction from the LBD to the DBD in PhlH (Fig. 8*A*). Dissociation of ligands from PhlH LBD leads to partial unfolding and deformation of the α7 helix and disrupts the H76-K144 hydrogen bond bridging the α7 and α4 helix. The N-terminal end of the α4 helix therefore moves inward. At the same time, the α6 helix bounces towards the ligand-binding tunnel and forces the C-terminal end of the α1 helix inward via the R124-F33/A34 interaction. These movements reposition the helix-turn-helix motif and result in the shortened distance between the α3 helices. Interestingly, in other TetR-family regulators such as DesT (37) and FadR (38, 39), a conserved basic residue (Arg or Lys) also exists in α6 helix and bridges the C-terminal end of the α1 helix *via* hydrogen-bonding in the DNA-bound conformation, yet in the ligand-bound conformation, this interaction is disrupted (Fig. 8*B*). Therefore, it seems that our proposed signal transduction mechanism of PhlH can even be applied to other distantly related TetR-family regulators.

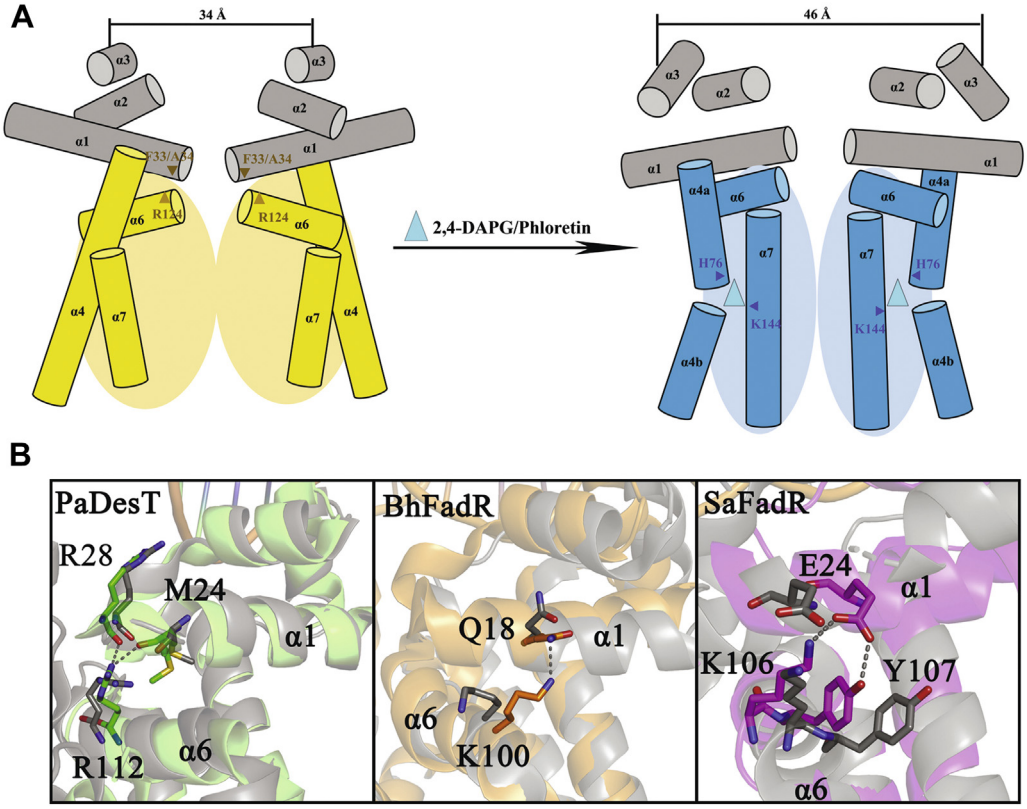

Figure 8. A putative transcriptional regulation mechanism of PhlH. *A*, a schematic representation illustrating the allosteric mechanism of closed to open conformational transition for PhlH. *B*, a conserved basic residue (Arg or Lys) also exists in α6 helix in other TetR-family regulators such as PaDesT (PDB code: 3LSJ and 3LSP), BhFadR (PDB code: 5GPC and 5GP9), and SaFadR (PDB code: 6EL2 and 6EN8) and bridges the C-terminal end of the α1 helix *via* hydrogen bonding in the DNA-bound conformation (*green*, *orange*, and *magenta*), yet in the ligand-bound conformation (*grays*), these interactions are disrupted. 2,4-DAPG, 2,4-diacetylphloroglucinol.

A large proportion of TetR-family members regulate efflux pumps and transporters involved in decreasing the intracellular concentration of certain toxic xenobiotics (26). However, several TetR-family regulators in Actinobacteria were characterized to perceive diffusible bacterial hormones such as γ-butyrolactone and methylenomycin furans and induce the expression of specialized metabolite biosynthetic gene clusters((40, 41)). For *Pseudomonas* PhlH, previous work established that it can sense 2,4-DAPG and plant flavonoids to induce the expression of 2,4-DAPG hydrolase, leading to a halt of 2,4-DAPG biosynthesis (20, 21). Our proteomics data indicated that PhlH also positively regulates fatty acid β-dation and biosynthesis of mupirocin, but negatively regulates biosynthesis of pyoverdine. As β-oxidation provides abundant acetyl-CoA molecules, which are building blocks of mupirocin (42), it is plausible that PhlH inhibits β-oxidation, resulting in a reduction in the intracellular acetyl-CoA levels and decreased mupirocin biosynthesis. On the other hand, pyoverdine biosynthesis requires myristic/myristoleic acid as the precursor (43), inhibition of β-oxidation is likely to allow myristic/myristoleic acid to escape the β-oxidation pathway and be shuttled into pyoverdine production. Since PhlH senses both the bacterial 2,4-DAPG and plant flavonoids, it is tempting to speculate that these signals, which signify high local density of the bacterial population or close proximity to plant roots, could advise *P. fluorescens* to secrete more pyoverdine siderophores for iron competition while lowering metabolic burdens by decreasing biosynthesis of antibiotic metabolites.

Experimental procedures

Cloning, expression, and purification

The *phlH* gene was amplified by PCR from *P. fluorescens* 2P24 (GenBank accession number DQ083928) and cloned into the modified pET28a vector (Novagene) which contains an N-terminal 6 × His tag. The cloning junctions were confirmed by DNA sequencing. Each recombinant plasmid was transformed into the *E. coli* Rosetta (DE3) strain (Novagen). Cells were grown at 37 °C in Luria Bertani medium containing 100 μg/ml kanamycin and 40 μg/ml chloramphenicol. Expression of PhlH was induced at an A_{600nm} of 0.8 by adding 0.2 mM isopropyl-β-D-1-thiogalactopyranoside followed by incubation at 16 °C for 20 h. The cells were harvested and sonicated in 20 mM Tris-HCl buffer pH 8.0 containing 100 mM NaCl in an ice-water bath. After centrifugation, the His-tagged fusion proteins were isolated with Ni-NTA affinity column (GE Healthcare) and further purified by gel filtration (Superdex 75, GE Healthcare) in a buffer containing 20 mM Tris-HCl pH 8.0, 100 mM NaCl. The eluted proteins were collected, concentrated using centrifugal ultrafiltration for further study. The PhlH mutants were obtained by site-directed mutagenesis using the plasmid encoding the

full-length PhlH as a template, overexpressed, and purified the same way as the WT protein. The selenomethionyl-PhlH (Se-PhlH) protein was overexpressed in *E. coli* strain B834 (DE3). Transformed cells were grown at 37 °C in SeMet medium (M9 medium supplemented with 60 μg/ml SeMet and other amino acids at 100 μg/ml) to an $A_{600\ nm}$ of 0.8 and then induced with 0.2 mM isopropyl-β-D-1-thiogalactopyranoside for another 4 h. SeMet substituted and mutant PhlH proteins were purified using the same protocol used for the native protein. The bacterial strains and primers used in this study were listed in Tables S2 and S3 respectively.

Crystallization and data collection

The purified native and Se-PhlH were concentrated by ultrafiltration (Millipore Amicon) to 20 mg/ml. Initial crystal screening was set up with Crystal Screen, Crystal Screen 2, and PEG/Ion Screen reagent kits (Hampton Research) at 16 °C by using the hanging-drop vapor-diffusion method. Crystals appeared within 4 weeks. Further crystal optimization experiments were performed by systematic variation of the precipitant concentration and protein concentration. The native and Se-PhlH crystals were produced by mixing 1 μl protein solution (∼20 mg/ml) and an equal volume of reservoir solution containing 10% w/v PEG 5000 MME, 12% v/v 1-propanol, 0.1 M MES pH 6.5, and incubating at 15 °C. The 2,4-DAPG-bound PhlH complexes were obtained by incubation of native PhlH (∼10 mg/ml) with 2,4-DAPG at a molar ratio of 1:2 for 30 min on ice. Crystallization of 2,4-DAPG-bound PhlH was performed at 16 °C using the hanging-drop vapor diffusion method. The appropriate crystals of 2,4-DAPG-bound PhlH were obtained from the reservoir solution of 2.8 M sodium chloride, 0.1 M sodium acetate trihydrate pH 4.7 after 2 weeks.

The crystals were harvested using cryoloops and immersed briefly in a cryoprotectant solution consisting of 80% (v/v) reservoir solution and 20% (v/v) glycerol. The crystals were subsequently flash-cooled and stored in liquid nitrogen and transferred to beamline BL17U1 and BL18U1 of the SSRF (Shanghai Synchrotron Radiation Facility) (44) for X-ray diffraction analysis and data collection. The dataset of Se-PhlH and 2,4-DAPG-bound PhlH were processed using HKL2000. Crystals of SeMet-derived PhlH and 2,4-DAPG-bound PhlH belong to $P4_12_12$ and $H32$, respectively. Table S4 gives a summary of the data collection statistics.

Structure determination and refinement

The crystal structure of Se-PhlH was determined using single-wavelength anomalous dispersion phasing method at a resolution of 2.4 Å. The AutoSol program implemented in PHENIX was used to locate the selenium atoms (45). Automatic model building was carried out using Autobuild in PHENIX (45). The resultant model was refined using the maximum likelihood method implemented in REFMAC5 as part of the CCP4i program suite (46) and the PHENIX program refinement (45) and rebuilt interactively using the program COOT (47). The structure of 2,4-DAPG-bound PhlH was determined by the molecular replacement method using the Se-PhlH structure as the search model. The final structure was solved at a higher resolution of 2.1 Å. The model was refined using the same method as the Se-PhlH structure. Both the structures were assessed with MolProbity (48), and the Ramachandran outliers were less than 1% in the final refined structures. Crystallographic parameters are listed in Table S4. All structure figures were prepared with PyMOL[50].

Electrophoretic mobility shift assay

6-carboxyfluorescein–labeled DNA fragments were obtained by annealing primers. The DNA fragments were added at a concentration of 0.2 μM and incubated at room temperature for 10 min with proteins of WT and mutated PhlH in a buffer containing 0 mM Tris-HCl at pH 8.0, 0.5 mM $MgCl_2$, 6 mM KCl, 0.1 % (vol/vol) glycerol, 5 mM EDTA, and 1 mM DTT and 3 μM of human serum albumin in a total volume of 20 μl. Reactions were prepared by adding 2,4-DAPG or phloretin to a final concentration of 0 to 50 μM or 0 to 500 μM. After incubation for 30 min at 25 °C, the mixtures were directly subjected to 6% native PAGE with 1 × Tris acetate-EDTA buffer. Electrophoresis was performed at 80 V, 4 °C in an ice-cold bath. For 6-carboxyfluorescein–labeled probes, the images were collected and analyzed on a Typhoon FLA-9500 imaging system (GE Healthcare).

Isothermal titration calorimetry

ITC experiments were performed at 25 °C employing a MicroCal iTC200 instrument (GE Healthcare). All WT and mutant samples and 2,4-DAPG were dissolved in a buffer containing 20 mM Tris-HCl pH 8.0, 100 mM NaCl, 0.5 % (vol/vol) DMSO, and degassed before use. The sample cell was loaded with 220 μl protein samples at 0.05 to 0.1 mM, whereas the injection syringe was loaded with 40 μl 2,4-DAPG at 0.5 to 1 mM. An initial 0.4 μl injection, which was subsequently removed during data analysis, was followed by 19 injections of 2.0 μl each. These injections were spaced at 2 min intervals. Additionally, heats of dilution were determined by titrating the 2,4-DAPG into a solution buffer (20 mM Tris-HCl pH 8.0, 100 mM NaCl, 0.5 % (vol/vol) DMSO) and subtracted from the raw titration data. Analyses of all data were performed with MicroCal Origin software accompanying the ITC instrument.

Total protein extraction, digestion, and mass spectrometry analysis

Bacterial cells of the WT *P. fluorescens* 2p24 and Δ*phlH* were cultured in KB broth to the early stationary phase and collected by centrifugation. The cells were lysed, and the protein was reduced and alkylated by heating at 95 °C for 10 min as previously described (49). A 1:10 dilution of the resulting mixture was made with the dilution buffer (25 mM Tris-HCl, pH 8.5, 10% acetonitrile) and digested with sequencing grade trypsin at 37 °C overnight. Peptides were acidified with 5% trifluoroacetic acid and loaded onto a C18-column equilibrated with methanol and 0.2% acetic acid. Peptides were then washed three times with 0.2% acetic acid,

eluted with the buffer containing 80% acetonitrile and 0.2% acetic acid, and dried using a SpeedVac centrifuge at 40 °C. Peptides were dissolved in 0.1% FA, and approximately 1 μg of peptides were loaded for a 120-min gradient MS analysis. An in-house packed 25-cm column with a 75-μm inner diameter (1.9 μm C18 resin) was used to separate the peptides. Liquid chromatography was performed with an EASY-nLC 1000 ultra-high pressure system (Thermo Fisher Scientific), coupled to the Orbitrap Fusion Lumos mass spectrometer (Thermo Scientific). Raw data files were analyzed with MaxQuant software (50), and peak lists were searched in the FASTA database of *P. fluorescens* 2P24. Oxidation on methionine was set as variable modifications, and cysteine carbamidomethylation was set as a fixed modification. Gene Ontology enrichment and statistical analysis were carried out with clusterProfiler software (51). Student's *t* test was used to determine the significance of protein differential expression, and Fisher's-exact test was used for the functional enrichment analysis. In total, 1590 proteins were identified with 1% FDR. Hierarchical clustering using z-scored intensities of the proteins quantified with high confidence ($p < 0.05$) showed that five-replicate samples of WT and Δ*phlH* were correctly clustered together (Fig. S5), indicating the high reproducibility of our quantification.

MD simulation and SSN analysis

MD simulations were carried out using the AMBER16 software package (52). The general AMBER force field (GAFF) (53) and ff14SB force field (54) were used for the PhlH protein and 2,4-DAPG ligand, respectively. Atom types and AM1-BCC atomic charges of indole were calculated using antechamber module of AMBER16 package. The missing hydrogen atoms were added by using the LEaP module of AMBER16 software, and the simulation systems were solvated in a cubic TIP3P water box, which extended a 10 Å distance from the box surface to solute. Several counter ions were added for neutralization. The energy of the simulation systems was minimized to eliminate the possible bumps between solute and water. Subsequently, the two systems were heated gradually in the NVT ensemble from 0 to 300 K with a weak restraint (k = 5 kcal mol^{-1} $Å^{-2}$). Finally, the 1000-ns production MD simulation was conducted in NPT ensembles under the temperature of 310 K and the pressure of 1 atm. For the GaMD simulation, the GPU version of the GaMD module was used (28). Briefly, a 100-ns conventional MD simulation was performed to collect the potential statistics and after adding the boost potential, a 1000-ns GaMD production simulation was performed. In all the simulations, *Particle-mesh Ewald* (55) was used to handle the long-range electrostatic interaction and analysis of MD trajectories was carried out with the *cpptraj* module.

To investigate the distribution of PhlH homologs in bacteria, we retrieved 1000 homologous sequences of PhlH from the UniProt database with and a BLAST query e-value of 10^{-5} and created a SSN using the enzyme similarity tool–EST server (https://efi.igb.illinois.edu/efi-est/). To optimize cluster separation and visual presentation, the SSN was filtered to a threshold of approximately 39% sequence identity.

Data availability

The MS raw files and proteome sequences of *P. fluorescens* 2P24 have been deposited to the ProteomeXchange Consortium *via* the PRIDE partner repository with the data set identifier PXD025403 (http://www.proteomexchange.org) (Vizcaino *et al.*, 2016). The coordinates and structure factors have been deposited in the Protein Data Bank under the accession code 7E1L and 7E1N.

Supporting information—This article contains supporting information (20).

Acknowledgments—We thank the Core Facility of the School of Life Sciences of Lanzhou University for proteomic data collection, SSRF beamline BL17U1 and BL18U1 for synchrotron data collection. We also thank the staff for providing technical support by using the facility of the Institute of Health Sciences and Technology of Anhui University.

Author contributions—Y-.X. H., H. G., and N. Z. conceptualization, Y-.X. H., H. G., J. W., S. Z., L. Q. Z., and N. Z. methodology; Y-.X. H., H. G., and N. Z. supervision. Y-.X. H., N. Z., and H. G. formal analysis. Y-.X. H., N. Z., and H. G. writing-original draft. J. W., S. Z., M. Y., P. Z., H. G., M. W., N. Z., M. Y., J. L., H. X., M. L. K., and Y-.X. H. investigation. Y-.X. H., H. G., N. Z., M. L. K., X. T., L. Q. Z., J. W., S. Z., M. Y., P. Z., H. G., M. W., N. Z., J. L., H. X., writing-review and editing; N. Z., J. W., S. Z., H. X., M. W., Y-.X. H., and H. G. software, N. Z., Y-.X. H., and H. G. project administration; N. Z., Y-.X. H., and H. G. funding acquisition; J. W., S. Z., and M. Y. data curation; S. Z., M. Y., H. X., and J. L. validation; P. Z. and L. Q. Z. recources.

Funding and additional information—This work was supported by the grants from the National Natural Science Foundation of China (grant Nos. 31970103 and 31971422), Key Research and Development Plan Project of Anhui Province (grant No. 202004a06020035), and Anhui Natural Science Foundation of China (grant No. 2108085MC76).

Conflict of interest—The authors declare that they have no conflicts of interest with the contents of this article.

Abbreviations—The abbreviations used are: 2,4-DAPG, 2,4-diacetylphloroglucinol; LBD, ligand-binding domain; DBD, DNA-binding domain; PGPR, plant growth–promoting rhizobacteria; RMSD, root mean square deviation; ITC, isothermal titration calorimetry; EMSAs, electrophoretic mobility shift assays; MD, molecular dynamics; PMF, potential of mean force; GaMD, gaussian accelerated molecular dynamics; SSN, sequence similarity network.

References

1. Tengerdy, R. P., and Szakács, G. (1998) Perspectives in agrobiotechnology. *J. Biotechnol.* **66**, 91–99
2. Haas, D., and Défago, G. (2005) Biological control of soil-borne pathogens by fluorescent pseudomonads. *Nat. Rev. Microbiol.* **3**, 307–319
3. Siddiqui, Z. A. (2006) *PGPR: Biocontrol and Biofertilization*, Springer, Dordrecht

4. Haas, D., and Keel, C. (2003) Regulation of antibiotic production in root-colonizing Peudomonas spp. And relevance for biological control of plant disease. *Annu. Rev. Phytopathol.* **41**, 117–153
5. Lucke, M., Correa, M. G., and Levy, A. (2020) The role of secretion systems, effectors, and secondary metabolites of beneficial rhizobacteria in interactions with plants and microbes. *Front. Plant Sci.* **11**, 589416
6. Diggle, S. P., Griffin, A. S., Campbell, G. S., and West, S. A. (2007) Cooperation and conflict in quorum-sensing bacterial populations. *Nature* **450**, 411–414
7. Tsunematsu, Y., Ishikawa, N., Wakana, D., Goda, Y., Noguchi, H., Moriya, H., *et al.* (2013) Distinct mechanisms for spiro-carbon formation reveal biosynthetic pathway crosstalk. *Nat. Chem. Biol.* **9**, 818–825
8. El-Sayed, A. K., Hothersall, J., Cooper, S. M., Stephens, E., Simpson, T. J., and Thomas, C. M. (2003) Characterization of the mupirocin biosynthesis gene cluster from Pseudomonas fluorescens NCIMB 10586. *Chem. Biol.* **10**, 419–430
9. Haas, D., Blumer, C., and Keel, C. (2000) Biocontrol ability of fluorescent pseudomonads genetically dissected: importance of positive feedback regulation. *Curr. Opin. Biotechnol.* **11**, 290–297
10. Khan, S. R., Mavrodi, D. V., Jog, G. J., Suga, H., Thomashow, L. S., and Farrand, S. K. (2005) Activation of the phz operon of Pseudomonas fluorescens 2-79 requires the LuxR homolog PhzR, N-(3-OH-Hexanoyl)-L-homoserine lactone produced by the LuxI homolog PhzI, and a cis-acting phz box. *J. Bacteriol.* **187**, 6517–6527
11. Latour, X. (2020) The evanescent GacS signal. *Microorganisms*. https://doi.org/10.3390/microorganisms8111746
12. Laville, J., Voisard, C., Keel, C., Maurhofer, M., Défago, G., and Haas, D. (1992) Global control in Pseudomonas fluorescens mediating antibiotic synthesis and suppression of black root rot of tobacco. *Proc. Natl. Acad. Sci. U. S. A.* **89**, 1562–1566
13. Raaijmakers, J. M., and Weller, D. M. (2001) Exploiting genotypic diversity of 2,4-diacetylphloroglucinol-producing Pseudomonas spp.: characterization of superior root-colonizing P. Fluorescens strain Q8r1-96. *Appl. Environ. Microbiol.* **67**, 2545–2554
14. Raaijmakers, J. M., and Weller, D. M. (1998) Natural plant protection by 2,4-diacetylphloroglucinol-producing Pseudomonas spp. In take-all decline soils. *Mol. Plant Microbe Interact.* **11**, 144–152
15. Bangera, M. G., and Thomashow, L. S. (1999) Identification and characterization of a gene cluster for synthesis of the polyketide antibiotic 2, 4-diacetylphloroglucinol from Pseudomonas fluorescens Q2-87. *J. Bacteriol.* **181**, 3155–3163
16. Achkar, J., Xian, M., Zhao, H., and Frost, J. W. (2005) Biosynthesis of phloroglucinol. *J. Am. Chem. Soc.* **127**, 5332–5333
17. Pavkov-Keller, T., Schmidt, N. G., Żądło-Dobrowolska, A., Kroutil, W., and Gruber, K. (2019) Structure and catalytic mechanism of a bacterial friedel-crafts acylase. *Chembiochem* **20**, 88–95
18. Abbas, A., McGuire, J. E., Crowley, D., Baysse, C., Dow, M., and O'Gara, F. (2004) The putative permease PhlE of Pseudomonas fluorescens F113 has a role in 2,4-diacetylphloroglucinol resistance and in general stress tolerance. *Microbiology* **150**, 2443–2450
19. Schnider-Keel, U., Seematter, A., Maurhofer, M., Blumer, C., Duffy, B., Gigot-Bonnefoy, C., *et al.* (2000) Autoinduction of 2,4-diacetylphloroglucinol biosynthesis in the biocontrol agent Pseudomonas fluorescens CHA0 and repression by the bacterial metabolites salicylate and pyoluteorin. *J. Bacteriol.* **182**, 1215–1225
20. Yan, X., Yang, R., Zhao, R.-X., Han, J.-T., Jia, W.-J., Li, D.-Y., *et al.* (2017) Transcriptional regulator PhlH modulates 2,4-diacetylphloroglucinol biosynthesis in response to the biosynthetic intermediate and end product. *Appl. Environ. Microbiol.* **83**, e01419-17
21. Yu, X.-Q., Yan, X., Zhang, M.-Y., Zhang, L.-Q., and He, Y.-X. (2020) Flavonoids repress the production of antifungal 2,4-DAPG but potentially facilitate root colonization of the rhizobacterium Pseudomonas fluorescens. *Environ. Microbiol.* **22**, 5073–5089
22. Ochsner, U. A., Wilderman, P. J., Vasil, A. I., and Vasil, M. L. (2002) GeneChip expression analysis of the iron starvation response in Pseudomonas aeruginosa: identification of novel pyoverdine biosynthesis genes. *Mol. Microbiol.* **45**, 1277–1287
23. Drake, E. J., Cao, J., Qu, J., Shah, M. B., Straubinger, R. M., and Gulick, A. M. (2007) The 1.8 A crystal structure of PA2412, an MbtH-like protein from the pyoverdine cluster of Pseudomonas aeruginosa. *J. Biol. Chem.* **282**, 20425–20434
24. Wells, G., Palethorpe, S., and Pesci, E. C. (2017) PsrA controls the synthesis of the Pseudomonas aeruginosa quinolone signal *via* repression of the FadE homolog, PA0506. *PLoS One* **12**, e0189331
25. Yu, Z., Reichheld, S. E., Savchenko, A., Parkinson, J., and Davidson, A. R. (2010) A comprehensive analysis of structural and sequence conservation in the TetR family transcriptional regulators. *J. Mol. Biol.* **400**, 847–864
26. Cuthbertson, L., and Nodwell, J. R. (2013) The TetR family of regulators. *Microbiol. Mol. Biol. Rev.* **77**, 440–475
27. Lara, J., Diacovich, L., Trajtenberg, F., Larrieux, N., Malchiodi, E. L., Fernández, M. M., *et al.* (2020) Mycobacterium tuberculosis FasR senses long fatty acyl-CoA through a tunnel and a hydrophobic transmission spine. *Nat. Commun.* **11**, 3703
28. Miao, Y., Feher, V. A., and McCammon, J. A. (2015) Gaussian accelerated molecular dynamics: unconstrained enhanced sampling and free energy calculation. *J. Chem. Theor. Comput.* **11**, 3584–3595
29. Gerlt, J. A., Bouvier, J. T., Davidson, D. B., Imker, H. J., Sadkhin, B., Slater, D. R., *et al.* (2015) Enzyme function initiative-enzyme similarity tool (EFI-EST): a web tool for generating protein sequence similarity networks. *Biochim. Biophys. Acta* **1854**, 1019–1037
30. Huang, X., Zhu, D., Ge, Y., Hu, H., Zhang, X., and Xu, Y. (2004) Identification and characterization of pltZ, a gene involved in the repression of pyoluteorin biosynthesis in Pseudomonas sp. M18. *FEMS Microbiol. Lett.* **232**, 197–202
31. Guo, D.-D., Luo, L.-M., Ma, H.-L., Zhang, S.-P., Xu, H., Zhang, H., *et al.* (2020) The regulator PltZ regulates a putative ABC transporter system PltIJKNOP of Pseudomonas aeruginosa ATCC 27853 in response to the antimicrobial 2,4-diacetylphloroglucinol. *Front. Microbiol.* **11**, 1423
32. Morris, J. H., Apeltsin, L., Newman, A. M., Baumbach, J., Wittkop, T., Su, G., *et al.* (2011) clusterMaker: a multi-algorithm clustering plugin for Cytoscape. *BMC Bioinform.* **12**, 436
33. Williams, M. A., and Ladbury, J. E. (2008) Hydrogen bonds in protein-ligand complexes. *Protein Sci. Encycl.* https://doi.org/10.1002/9783527610754.pl02
34. Alguel, Y., Meng, C., Terán, W., Krell, T., Ramos, J. L., Gallegos, M.-T., *et al.* (2007) Crystal structures of multidrug binding protein TtgR in complex with antibiotics and plant antimicrobials. *J. Mol. Biol.* **369**, 829–840
35. Frénois, F., Engohang-Ndong, J., Locht, C., Baulard, A. R., and Villeret, V. (2004) Structure of EthR in a ligand bound conformation reveals therapeutic perspectives against tuberculosis. *Mol. Cell.* **16**, 301–307
36. Schumacher, M. A., Miller, M. C., Grkovic, S., Brown, M. H., Skurray, R. A., and Brennan, R. G. (2001) Structural mechanisms of QacR induction and multidrug recognition. *Science* **294**, 2158–2163
37. Miller, D. J., Zhang, Y.-M., Subramanian, C., Rock, C. O., and White, S. W. (2010) Structural basis for the transcriptional regulation of membrane lipid homeostasis. *Nat. Struct. Mol. Biol.* **17**, 971–975
38. Wang, K., Sybers, D., Maklad, H. R., Lemmens, L., Lewyllie, C., Zhou, X., *et al.* (2019) A TetR-family transcription factor regulates fatty acid metabolism in the archaeal model organism Sulfolobus acidocaldarius. *Nat. Commun.* **10**, 1542
39. Yeo, H. K., Park, Y. W., and Lee, J. Y. (2017) Structural basis of operator sites recognition and effector binding in the TetR family transcription regulator FadR. *Nucl. Acids Res.* **45**, 4244–4254
40. Zhou, S., Bhukya, H., Malet, N., Harrison, P. J., Rea, D., Belousoff, M. J., *et al.* (2021) Molecular basis for control of antibiotic production by a bacterial hormone. *Nature* **590**, 463–467
41. Kapoor, I., Olivares, P., and Nair, S. K. (2020) Biochemical basis for the regulation of biosynthesis of antiparasitics by bacterial hormones. *Elife* **9**, e57824
42. Gurney, R., and Thomas, C. M. (2011) Mupirocin: biosynthesis, special features and applications of an antibiotic from a gram-negative bacterium. *Appl. Microbiol. Biotechnol.* **90**, 11–21
43. Hannauer, M., Schäfer, M., Hoegy, F., Gizzi, P., Wehrung, P., Mislin, G. L. A., *et al.* (2012) Biosynthesis of the pyoverdine siderophore of Pseudomonas aeruginosa involves precursors with a myristic or a myristoleic acid chain. *FEBS Lett.* **586**, 96–101

44. Wang, Z., Pan, Q., Yang, L., Zhou, H., Xu, C., Yu, F., *et al.* (2016) Automatic crystal centring procedure at the SSRF macromolecular crystallography beamline. *J. Synchrotron Radiat.* **23**, 1323–1332
45. Liebschner, D., Afonine, P. V., Baker, M. L., Bunkóczi, G., Chen, V. B., Croll, T. I., *et al.* (2019) Macromolecular structure determination using X-rays, neutrons and electrons: recent developments in phenix. *Acta Crystallogr. D Struct. Biol.* **75**, 861–877
46. Murshudov, G. N., Skubák, P., Lebedev, A. A., Pannu, N. S., Steiner, R. A., Nicholls, R. A., *et al.* (2011) REFMAC5 for the refinement of macromolecular crystal structures. *Acta Crystallogr. D Biol. Crystallogr.* **67**, 355–367
47. Emsley, P., and Cowtan, K. (2004) Coot: model-building tools for molecular graphics. *Acta Crystallogr. D Biol. Crystallogr.* **60**, 2126–2132
48. Chen, V. B., Arendall, W. B., 3rd, Headd, J. J., Keedy, D. A., Immormino, R. M., Kapral, G. J., *et al.* (2010) MolProbity: all-atom structure validation for macromolecular crystallography. *Acta Crystallogr. D Biol. Crystallogr.* **66**, 12–21
49. Wang, Y., Zhang, S.-P., Zhang, M.-Y., Kempher, M. L., Guo, D.-D., Han, J.-T., *et al.* (2019) The antitoxin MqsA homologue in Pseudomonas fluorescens 2P24 has a rewired regulatory circuit through evolution. *Environ. Microbiol.* **21**, 1740–1756
50. Tyanova, S., Temu, T., and Cox, J. (2016) The MaxQuant computational platform for mass spectrometry-based shotgun proteomics. *Nat. Protoc.* **11**, 2301–2319
51. Yu, G., Wang, L.-G., Han, Y., and He, Q.-Y. (2012) clusterProfiler: an R package for comparing biological themes among gene clusters. *OMICS* **16**, 284–287
52. Case, D. A., Cheatham, T. E., 3rd, Darden, T., Gohlke, H., Luo, R., Merz, K. M., Jr., *et al.* (2005) The Amber biomolecular simulation programs. *J. Comput. Chem.* **26**, 1668–1688
53. Hornak, V., Abel, R., Okur, A., Strockbine, B., Roitberg, A., and Simmerling, C. (2006) Comparison of multiple Amber force fields and development of improved protein backbone parameters. *Proteins* **65**, 712–725
54. Wang, J., Wolf, R. M., Caldwell, J. W., Kollman, P. A., and Case, D. A. (2004) Development and testing of a general amber force field. *J. Comput. Chem.* **25**, 1157–1174
55. Darden, T., York, D., and Pedersen, L. (1993) Particle mesh Ewald: an N·log(N) method for Ewald sums in large systems. *J. Chem. Phys.* **98**, 10089